Journal of Ambient Intelligence and Humanized Computing (2021) 12:635–652
https://doi.org/10.1007/s12652-020-02046-3

ORIGINAL RESEARCH

Enhanced F-OFDM candidate for 5G applications

Montadar Abas Taher[1] · **Hussein Sultan Radhi**[2] · **Ahmed K. Jameil**[1]

Received: 19 October 2019 / Accepted: 25 April 2020 / Published online: 21 May 2020

Abstract
The demand for high data rate, the generation of Internet of Things (IoT), and various Machine Type Communications (MTC) emerged for a new transmission phenomenon. In other words, it is substantial to communicate without synchronization, or synchronization overhead, with mixed signal types. such specifications cannot be covered by the Fourth Generation (4G) systems, which is based on Cyclic Prefix Orthogonal Frequency Division Multiplexing (CP-OFDM). However, to achieve the specifications of the next generation system, numerous waveform replacements for the CP–OFDM were suggested, Filter Bank Multi–Carrier (FBMC), Generalized Frequency Division Multiplexing (GFDM), Universal Filtered Multi–Carrier (UFMC), and Filtered OFDM (F–OFDM). The filter design occupies essential part in these replacements, thus, in this paper, novel filters are introduced where simulation results show that the proposed filters outperform previous designs in terms of spectral efficiency improved dramatically by releasing the synchronization overhead.

Keywords 4G · 5G · CP-OFDM · FBMC · Filter design · Filtered-OFDM (f-OFDM) · Time-frequency localization · UFMC · UF-OFDM

1 Introduction

With the improvement of innovation, new requests for data transmission have represented an uncommon test for the cutting edge cell framework. Other than the customary voice and information benefits over cell phones, fifth generation (5G) system is additionally anticipated that would bolster traffics that are in a general sense unique in relation to the conventional ones, for example, machine type communication (MTC), which uses very short messages, and the internet of things (IoT) (Andrews et al. 2014). To address the coming difficulties (Banelli et al. 2014), a fundamental procedure is to use adaptable waveforms. In 5G systems, a principal necessity of the waveform configuration is to help offbeat transmission with a specific end goal to maintain a strategic distance from the substantial overhead of synchronization signalling needed by huge terminals (Andrews et al. 2014; Farhang-Boroujeny and Yuen 2010; Zhang et al. 2014; Schwarz and Rupp 2016; Schwarz et al. 2017; Schaich et al. 2014). In fourth generation (4G) systems, the employed modulation and access technique is the cyclic prefix orthogonal frequency division multiplexing (CP-OFDM), in spite of that, OFDM can barely meet the above necessity since the orthogonality among sub-carriers can't be kept up in eccentric/asynchronous transmission. Hence, out-of-band (OOB) emission will leads to unadorned adjacent channel interference (ACI) (Liu et al. 2017). The synchronization overhead, on the other hand, will degrade the latency and increases the consumption of power; meanwhile, MTC requires to be driven by batteries, which must last for a long lifetime (Wild wt al. 2014).

Furthermore, Notwithstanding the asynchronism of transmission, the time-domain localization property in 5G waveforms is mandatory, so as to support the required latency and short message transmission (Schaich et al. 2014). Hence, in order to qualify the waveform of 5G systems, filtered signals have been broadly contemplated as of late. That is, because

✉ Montadar Abas Taher
montadar@ieee.org

Hussein Sultan Radhi
hussein1957.hs@engineering.uodiyala.edu.iq

Ahmed K. Jameil
ahmedjameil@engineering.uodiyala.edu.iq

[1] Department of Communications Engineering, College of Engineering, University of Diyala, Baqubah 32001, Diyala, Iraq

[2] Department of Computer Engineering, College of Engineering, University of Diyala, Baqubah 32001, Diyala, Iraq

of the capacity to provide asynchronous transmission by filtered waveforms, which reduces the OOB emission, suggested filter based waveforms outperforms OFDM (Banelli et al. 2014). These filtered waveforms can be classified into sub-carrier based filtering, sub-band based filtering, and full band based filtering. In sub-carrier filtering approach, filter-bank multi-carrier (FBMC) (Bellanger 2010) outperforms conventional CP-OFDM, which uses offset quadrature amplitude modulation (OQAM) (Schaich 2010; Lu et al. 2012; Bedoui and Et-tolba 2017), another sub-carrier filtering based waveform is the generalized frequency division multiplexing (GFDM) (Fettweis et al. 2009; Michailow et al. 2014). However, although good features obtained, the long tail of the filter impulse response degrades the latency, which is substantial property in 5G systems (Wang et al. 2014). One of the reported solutions for the long tail was given in (Bellanger 2010) but the latency was increased. One more disadvantage of FBMC is the loss of complex orthogonality, which causes inter-symbol-interference (Wild wt al. 2014; Lu et al. 2012; Cheng et al. 2016).

For the aforementioned shortcomings, the second kind, sub-band based filtered-waveforms, was put. This approach will configure the filter to cover a sub-band, wherein each sub-band multi sub-carriers, are available for transmission. In other words, the impulse response of the filter will be shorter than the case of per sub-carrier filter operation because of the wider filter bandwidth. To get deep understand our claim; let us give a short introduction about the configuration of the fourth generation LTE system. In general, LTE (4G) time-domain transmission coordinated as periods. Thus, each period, which is called frame, lasts for 10 ms. The one individual frame consists of ten sub-frames, equally occupies the period of the frame. Hence, one frame incorporates smaller pieces called sub-frames, each is 1 ms long, where each sub-frame subdivided equally into two time-slots. Time-slots, which are each is 0.5 ms long, are the main containers of the CP-OFDM symbols. Consequently, there will be six or seven CP-OFDM symbols in each one time-slot according to the duration of the cyclic prefix duration, which is decided by the transmission environments. Subsequently, the LTE transmission bandwidth capacities can be determined with respect to the total number of subcarriers utilized for transmission, where each group of twelve adjacent subcarriers constitutes the so-called physical resource block (PRB) or for convenience a resource block (RB). The RB is employed in the base station as a littlest member of resources allocated for transmission scheduling (Taher and Ahmed 2015; Taher et al. 2015).

According to the LTE configurations, each sub-band constitutes 12 sub-carriers, which is called a resource block (RB), hence the resource block filtered OFDM was introduced (Li et al. 2015, 2014). As a suggested candidate for 5G, the universal filtered multi-carrier (UFMC) was another suggestion (Schaich et al. 2014; Wild wt al. 2014; Wang et al. 2014; Wang et al. 2019), which also belongs to the sub-band based filtering category. In UFMC filtering operation achieved in the transmitter side only, then, only one filter is needed per sub-band at the transmitter only. The filter bandwidth can be increased more such that the whole bandwidth of the transmitted sub-bands, collectively, will be filtered at once. That is, only one filter at the transmitter will be employed. This kind of filtered signal called filtered-OFDM (F-OFDM) (Zhang et al. 2014; Abdoli et al. 2015; Ahmed et al. 2020). It is worth saying that both FBMC and F-OFDM are special cases of the UFMC, whereby reducing the filter size to one sub-carrier width; UFMC reduced to FBMC while increasing the filter width to the whole allocated bandwidth, UFMC becomes F-OFDM, thus the name universal filtered multi-carrier. This paper will focus on the F-OFDM only. This paper is organized as follows; in Sect. 2, the related work about F-OFDM will be introduced as state of the art, filter design using windowing and finite impulse response filter will be discussed in Sects. 3, 4 suggests new F-OFDM implementation using windows not used in the literature, as to the best knowledge of the author, the simulation results and discussions will be given in Sect. 5, while concluding remarks will be shown in Sect. 6.

2 Related work

In the next generation of wireless communication systems, 5G, different numerology have to be employed to support various MTC systems and IoT devices. These numerologies include sub-carrier-spacing, variable cyclic prefix, required time interval for transmission, etc. Furthermore, it is essential to relax the synchronization between base station and devices, where tough signalling overhead will be available for data transmission. To achieve these requirements, the waveform should be flexible to configure it according to the type of traffic. The CP-OFDM uses a waveform that is a rectangular-pulse shaped in time-domain, which corresponds to sinc−shape in the frequency domain. However, the major downside of the sinc−function is that its side-lobes decay as slowly as $1/f$, where f is the frequency. sinc−function side-lobes prevent the frequency localization, which leads to loss of the coexistence with adjacent services (Abdoli et al. 2015). Furthermore, a drawback caused by sinc−side-lobes is the requirement of tight synchronizations both in time and frequency domains.

Thus, to relax the synchronization conditions, different kinds of waveforms have been introduced in the literature as stated in Sect. 1. however, the main objective to get asynchronous transmission is to avoid the OOB emission (Cheng et al. 2016; Wang et al. 2017; An et al. 2017). F-OFDM has gained a lot of attention in the literature; in (Abdoli

et al. 2015), the authors suggested F-OFDM to eliminate the long tail impulse response of the traditional CP-OFDM, furthermore, they suggested asynchronous multi-user system using F-OFDM. Many advantages can be reported for the F-OFDM such as; asynchronous communication, multiple input multiple output (MIMO) antenna capability, band configuration for different numerology, asynchronous multiple access, and easy system implementation. Although UFMC can accommodate same features of F-OFDM, F-OFDM outperforms UFMC (Zhang et al. 2014; Li et al. 2015; Abdoli et al. 2015). The UFMC filter length limited to the zero-padding length to get rid of the inter-symbol interference, while the filter length of the F-OFDM may exceed the CP length, so as to permit superior trade-off between time and frequency localization.

Nevertheless, CP-OFDM used pulse shaping to produce enhanced spectrum-localization, while the proposed F-OFDM suppresses the OOB emission which produces superior localization. Because of the high OOB emission from the traditional CP-OFDM, guard band becomes compulsory, as a consequence, a recognized spectrum waste. In 4G LTE systems, about 10% of the allocated bandwidth used as guard band (5G–NR 2019). Various approaches were introduced to achieve time-frequency localization trade-off. In order to avoid the *sinc*–function in the frequency domain, another pulse shape has to be used. Abdoli et al. (2015) used as simple as real-time filter generation, which is a truncation of the prototype filter by windowing the impulse response of the filter, such as Hanning window. The Gaussian pulse, which has the same shape in time and frequency domains, can be used (Gokceli et al. 2018), but this pulse leaks in orthogonality, hence, inter-carrier interference (ICI) and ISI can be recognized significantly. Therefore, the waveform to be adopted should produce superior spectrum efficiency, time and frequency localization, and orthogonality between sub-carriers. Unfortunately, according to Gabor's theory (Bölcskei 2003), we cannot obtain all these features at the same time. That is, the waveform must be designed smartly to put good trade-off between the time and frequency localization, spectrum efficiency improvement over CP-OFDM, and to keep the orthogonality. Bazzi et al. (2015) designed a filter using the same approach of (Abdoli et al. 2015) but with a different window, which is Von Hann window, it was found that F-OFDM outperforms the FBMC and UFMC.

That is, to eliminate the interference between consecutive sub-bands, filtering is needed to diminish the OOB transmission to a controlled level. More details about F-OFDM was introduced by Wu et al. (2016), where a practical field test was accomplished and proved that F-OFDM outperforms the CP-OFDM. It is shown in (Wu et al. 2016) that asynchronous subbands can be used with ignored interference between neighbouring sub-bands. Nevertheless, F-OFDM releases the usage of guard bands, this leads to relaxing more sub-carriers for useful data transmission, thus, increased spectrum efficiency (Zhang et al. 2014). Hu and Armada provided a comparison between two different numerologies, namely MTC and traditional voice signals, where the results proved the capability of F-OFDM to support mixed numerologies (Hu and Armada 2016). Another field test was conducted in (Wang et al. 2017) and it is shown that more than 7% increment in the throughput was achieved with negligible interference between adjacent sub-bands. The difference between the two field tests is that only up-link communication conducted in (Wu et al. 2016), while in (Wang et al. 2017) the communication was in the down-link. One more suggested methodology to reduce the OOB emission was discussed in (An et al. 2017), where windowing and filtering or filtering and windowing was achieved according to the location of filter and window. Hence in the next section, the design methodology will be shown with new windows will be introduced.

However, it is wealth to mention that there are two different delays, first; there is signal-processing delay, which is recognized at the receiving end, this signal processing delay depends on the processing power of the receiver such as foreword error correction, channel estimation and equalization. Thus, in F-OFDM as compared to CP-OFDM, the additional signal processing is the delay due to the spectrum-shaping filter; hence, this delay depends on the processing power of the receiving end. Second, as a baseline, CP-OFDM has T_{CP} which is the cyclic prefix duration consists of a copy of end data subcarriers appended to the beginning of the symbol. In F-OFDM, there are two portions of extra durations; at the start of the symbol of $T_{CP}/2$ and another $T_{CP}/2$ at the end of the symbol, that is, the extra delay, which is accepted by the designers (Huawei and HiSilicon 2016), in the F-OFDM is T_{CP} (Huawei and HiSilicon 2016).

In digital signal processing, window functions are used to stay away of the edge reactions due to splitting the signal to blocks. Hence, to get a middle way in between time and frequency domains resolutions, window functions are used, where window function has great impact on the signal's spectrum. Every window has to retain the following essential configurations: the window should be (in time-domain) (Andreas 2006); even, not negative, the main lobe at the origin while side lobes on the sides of the main lobe where the main lobe must be as skinny as possible and has the majority of the energy, and with respect to the main lobe the side lobe has to be shrink. In the history, there are a collection of windows such as but not limited to; rectangular, triangular, cosine family, Hann, truncated Taylor family, Hamming, raised-cosine family, Blackman, Blackman–Harris, Tukey, Dolph–Chebyshev, and Kaiser windows (Andreas 2006). In the next sections, we will explore some of these windows in deep as per the scope needs of this work.

3 Filter designing methodology

From the aforementioned notes in the previous section, F-OFDM performance, for superior time and frequency localization to improve the spectrum efficiency, depends mainly on the filter design. A technique which is simple, systematic, easy implementable on-line such as in the software defined radio (SDR), is the windowed−*sinc* method (Mitra and Kuo 2006). Note that the main goal of the filter utilization is to provide suitable attenuation at the stopband to make sure that the interference with neighbor subcarriers is insignificant, thus, the filter copes up with interference with other close spectrum (Huawei and HiSilicon 2016; Hammoodi et al. 2019; Taher 2019), in other words, the possibility of co-existence with other generations is possible such as with second generation (2G), third generation (3G) and 4G.

In the introduction, it was introduced the UFMC, FBMC, and F-OFDM, however, when the filter having all the filter is efficient when the spectrum having all bands of frequency or in other words, it will perform just like the last candidate, F-OFDM, where there is high stopband attenuation which will prevent the interference with other closed spectrum.

Actually, there are various well-defined windows, which make this filter design method sympathetic. Mathematically,

$$h(n) = h_r(n) \cdot w_n(n) \tag{1}$$

$h_r(n)$ is the required time-domain response of the filter. An ideal low-pass-filter (LPF) sinc response can be used (Hu and Armada 2016)

$$h_r(n) = \frac{1}{2\pi} \int_{-\omega_c}^{\omega_c} e^{j\omega n} d\omega = \frac{\sin(\omega_c n)}{\omega_c n} \tag{2}$$

where ω_c stands for the cut-off frequency. After the windowing operation, the resulted filter has to be shifted in the frequency domain (modulation property of the discrete-time Fourier transform (DTFT)) to be at the centre of the dedicated bandwidth. That is, the windowing of *sinc*−filter in the time domain will output ripple of frequencies near to the edge of the band, this is because of the Gibbs phenomenon (Mitra and Kuo 2006; Oppenheim et al. 2014). However, the ripple frequency can be eliminated if the allocated bandwidth extended for few sub-carriers at the transition edges, in this manner, the filter passes frequencies as flat as possible for the allocated sub-band, at the same time the filter's roll-off will begin at the designed edges of the sub-band. That is to say, filter design plays an essential role, for that reason, the filter design methodology should be smart by choosing an appropriate window function. Consequently, reduced OOB emission can be achieved, leading to improvement in the time and frequency localization significantly, therefore, the spectrum efficiency will be amended by releasing more bands, which will be used by the useful data, unlike the traditional CP-OFDM, accordingly, the data throughput increases. In (Weitkemper et al. 2016), the authors suggested making the filter size to be adaptable according to the used case of the numerology, however, this is possible with F-OFDM. A fast convolution to implement the digital filter for the F-OFDM was suggested in (Renfors et al. 2015) for filters with the short impulse response.

There are a variety of windows in the literature, each window type has its advantages and disadvantages. For instance, the simplest window is the rectangular-window, which is shown in Fig. 1 for a number of samples (length, L) equal to 31 points.

The rectangular window can be expressed as

$$w(n) = \begin{cases} 1, \text{ if } -\frac{L-1}{2} \le n \le \frac{L-1}{2}. \\ 0, \text{ otherwise.} \end{cases} \tag{3}$$

where L stands for the length of the window $w(n)$, odd in this discussion. The discrete time Fourier transform (DTFT) of $w(n)$ will depict the rectangular behaviour in the frequency domain

$$W(\omega) = DTFT(w(n)) = \sum_{n=-\infty}^{n=\infty} w(n) e^{-j\omega n} \tag{4}$$

with $\omega \in [-\pi, \pi)$, after some algebraic simplifications $W(\omega)$ becomes

$$W(\omega) = \text{sinc}(fL) \tag{5}$$

in other words, the zero-crossings appeared at multiple integers of $2\pi/L$, energy distribution of the symbol in time-domain, see Fig. 1, and are uniform. The CP-OFDM, which is employed in 4G LTE, adopted the rectangular window as a prototype filter to eliminate the effects of the ICI and

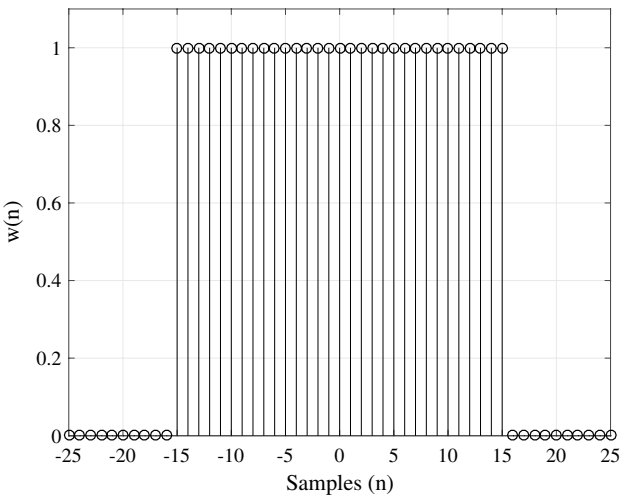

Fig. 1 Rectangular window of length $L = 31$

the ISI when passing the signal in time-invariant multipath channel. The big problem in the rectangular function is that it is not very well localized in the frequency domain. Fig. 2 shows the frequency response of the rectangular-function, which is reduced to sinc−function. From Fig. 2, it is obvious that the first side lobe is only $13dB$ below the main lobe and the side lobs are decreasing as slowly as $1/f$. Furthermore, it is shown that the rectangular window is not localized in the frequency domain. Therefore, it is not recommended for adoption in 5G systems.

Triangular function is another kind of windows, which is also known as Bartlett window, can be formulated as follows (Oppenheim et al. 2014): for the odd length of the window, (see Fig. 3)

$$w(n) = \begin{cases} \frac{2n}{L+1}, & \text{if } 1 \le n \le \frac{L+1}{2}. \\ 2 - \frac{2n}{L+1}, & \text{if } \frac{L+1}{2} + 1 \le n \le L. \end{cases} \tag{6}$$

and when the length of window is even,

$$w(n) = \begin{cases} \frac{2n-1}{L}, & \text{if } 1 \le n \le \frac{L}{2}. \\ 2 - \frac{2n-1}{L}, & \text{if } \frac{L}{2} + 1 \le n \le L. \end{cases} \tag{7}$$

The transform domain of the triangular window reduced to

$$W(\omega) = \left(\frac{L-1}{2}\right)^2 \text{sinc}^2(\omega) \tag{8}$$

On the other hand, it is evidently shown in Fig. 4 that the triangular function has a similar performance as that of the rectangular, where the first side lobe is only $13dB$ below the main window; therefore, it is not recommended to adopt the

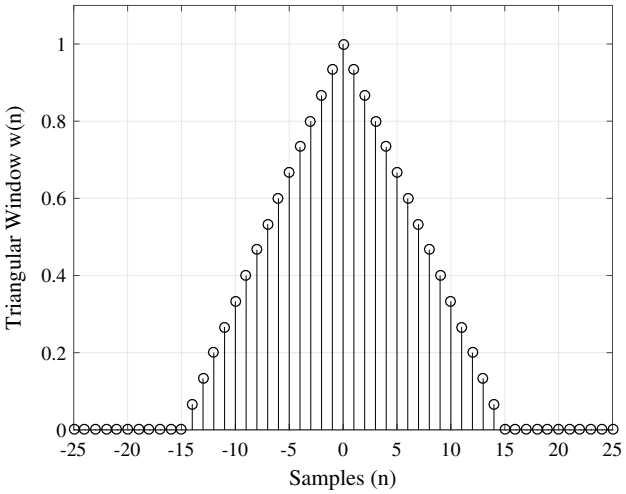

Fig. 3 Triangular function in the time domain

triangular prototype filter for the next generation of communication systems, 5G, as it was discussed in (Yang and Xu 2017), where a comparison for the implementation of the F-OFDM using triangular window, tapered cosine window, Hamming window, and Blackman–Harris window.

In Table 1 some common prototype filters are used by different researches, for instance, Chebyshev prototype filter implemented in (Cheng et al. 2016; An et al. 2017; Hu and Armada 2016), root-raised-cosine prototype filter employed in (Bedoui and Et-tolba 2017; Wang et al. 2017; Wu et al. 2016; Qiu et al. 2017; Iwabuchi et al. 2017), the Hanning prototype filter implemented in (Abdoli et al. 2015; Wang et al. 2017; Hu and Armada 2016), while Hamming prototype shown in (Cheng et al. 2016; Yang and Xu 2017), in (Cheng et al. 2016) the Kaiser prototype filter was compared

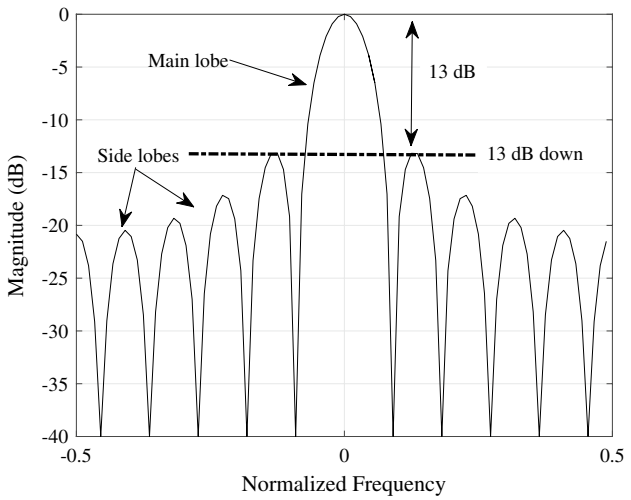

Fig. 2 Frequency domain of rectangular function represented as a sinc−function

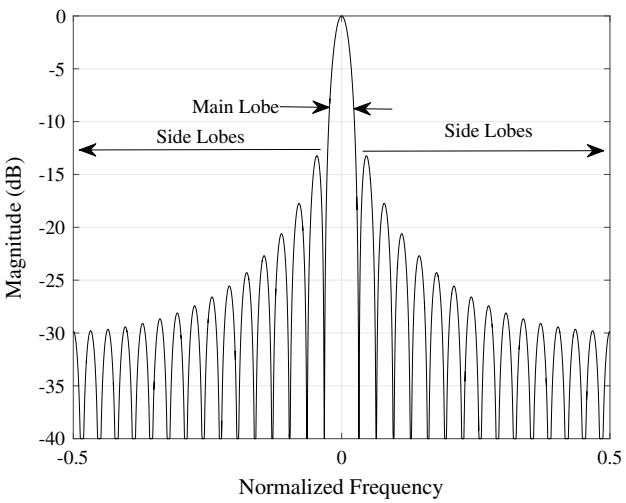

Fig. 4 Frequency domain representation of the triangular function

Table 1 Windows according to the utilization by researchers

#	Window name	References
1	Chebyshev	(Cheng et al. 2016; An et al. 2017; Hu and Armada 2016)
2	Root raised cosine	(Bedoui and Et-tolba 2017; Wang et al. 2017; Wu et al. 2016; Qiu et al. 2017; Iwabuchi et al. 2017)
3	Hanning	(Abdoli et al. 2015; Wang et al. 2017; Hu and Armada 2016)
4	Hamming	(Cheng et al. 2016; 5G–NR 2019)
5	Kaiser	(Cheng et al. 2016)
6	Blackman–Harris	(Cheng et al. 2016; Yang and Xu 2017)
7	Triangular	(Yang and Xu 2017)
8	Tapered cosine	(Yang and Xu 2017)

with other prototypes as shown in Table 1, the Blackman Harris found in (Cheng et al. 2016; Yang and Xu 2017), last but not least, the tapered cosine prototype filter was implemented in (Yang and Xu 2017). In fact, there was a comparative study of the performance of an F-OFDM based on Hanning and RRC prototype filters (Wang et al. 2017), in (Hu and Armada 2016) the Hanning and Chebyshev, in (Cheng et al. 2016) between Kaiser, Chebyshev, Hamming, and Blackman–Harris windows prototype filters, while in (Yang and Xu 2017) the comparison was conducted between the triangular, tapered cosine, Hamming, and the Blackman–Harris windows.

4 Proposed F-OFDM design

The F-OFDM transmitter part, Tx, visualization starts at the gathering of the data, to be processed for transmission, as binary data. Thus, the binary data will be mapped according to the baseband modulation order using either quadrature phase shift keying (QPSK) or multi-point quadrature amplitude modulation (M-QAM). At that juncture, the samples will be converted from serial to parallel (demultiplexing) to be ready for the N_i–points inverse discrete Fourier transform (IFFT), for efficient implementation. After the N_i–IFFT operations, the signal will be multiplexed, i.e., will be converted from parallel to serial, where a cyclic prefix will be added to each numerology (CP_i). At this instant, the filter operation as a final baseband operation will be conducted. Note that the discussion about baseband transmission, i.e., there is no radio frequency carrier as shown in Fig. 5a.

In Fig. 5b, the reverse operation of the Tx side is presented. That is, the Rx side of the F-OFDM gathers signal from the channel, firstly it filters back the signal using the same filter of the Tx side, removing the CP, convert the signal to parallel format, then the signal fed to the FFT operations to convert it to the frequency domain, to multiplex it to be ready for the de-mapping operation, to produce the binary data. Because of the F-OFDM has the same structure of the traditional CP-OFDM, the peak to average power ratio problem still exist, but this problem can be solved in different methods(Taher et al. 2014, 2013, 2015; Jawhar et al. 2019; Lavanya et al. 2020), furthermore, the channel estimation is another issue in multicarrier modulation schemes, which need to study the probability density function of the channel and how to cope up with the F-OFDM signal (Zhou et al. 2018), however, these problems are out of the scope of this paper.

In the literature, alternating windows have been designed by combining two or more windows in different manners (Harris 1978). The goal was to obtain window with narrower main lobe width and very low side-lobe levels. For instance, the convolution of two rectangular windows produces Bartlett window, the summation of a rectangular window with Hanning window gives Hamming window, furthermore, by convolving two half-extent triangular windows releases de la Valle–Poussin window (Harris 1978). Moreover, by multiplying frequency domain rectangular window with cosine lobe, or by time-domain convolution of cosine lobe with the rectangular window, announces for a new window called cosine-tapered window, which is known as Tukey window. If two windows of type cosine lobe, or half-duration, convolved together, Bohman window can be realized, in other words, the time domain multiplication of a triangular window with a cosine cycle is the Bohman window. Imaging the product of two windows, the first is the Hanning window and the second is the Poisson window, then the result is well-known window called Hanning–Poisson window (Harris 1978).

As in the literature, the convolution of two time-domain windows, $w_a(n)$ and $w_b(n)$, as stated in the last subsection, will be examined in this paper according to two scenarios. The first scenario is dedicated to a combination of two different windows, while the second scenario will be dedicated to a convolution of a window with itself. In other words, in the first scenario, $w_a(n) \neq w_b(n)$, and the second scenario achieves $w_a(n) = w_b(n) = w(n)$. Those scenarios will be realized in the following subsections.

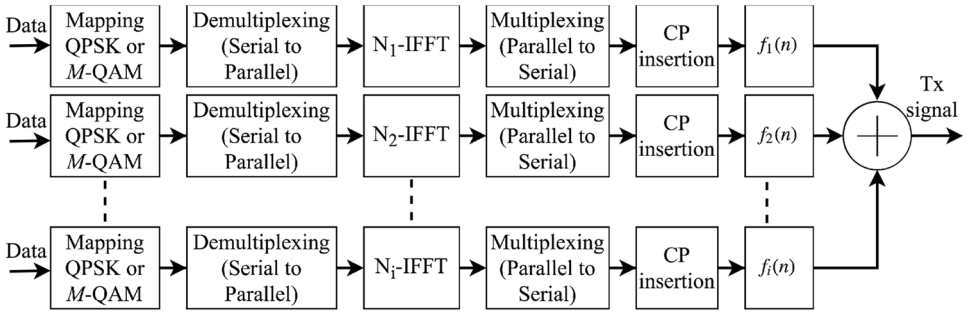

a Tx side of the F–OFDM transceiver.

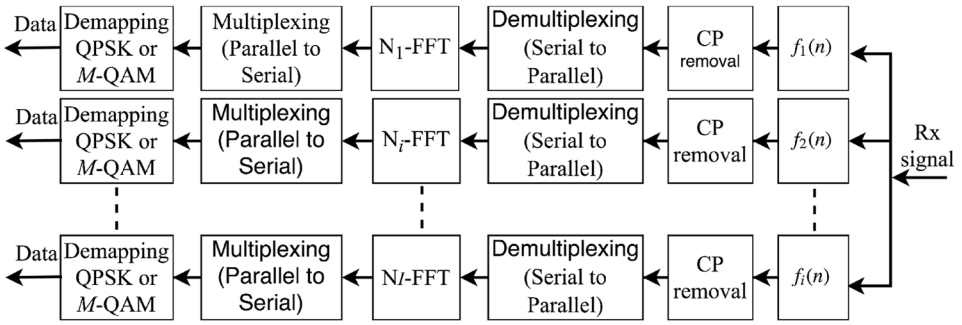

b Rx side of the F–OFDM transceiver.

Fig. 5 Tx side of the F-OFDM transceiver. Rx side of the F-OFDM transceiver.

Consider, for the first scenario, two different windows $w_a(n)$ as Hamming window and the second $w_b(n)$ as Hanning window,

$$w_a(n) = 0.54 - 0.46\cos\left(\frac{2\pi n}{P}\right) \tag{9}$$

where $P = L - 1$.

$$w_b(n) = 0.5 - 0.5\cos\left(\frac{2\pi n}{P}\right) \tag{10}$$

by convolving $w_a(n)$ and $w_b(n)$ in the frequency domain, both of half-extent, or by the product of them in the time domain, a new window released

$$w_{new}(n) = w_a(n) \cdot w_b(n) \tag{11}$$

in other words, the operation identified as windowing the first window, $w_a(n)$, by the second window, $w_b(n)$, which results in $w_{new}(n)$,

$$w_{new}(n) = \frac{77}{200} - \frac{1}{2}\cos\left(\frac{2\pi}{P}n\right) + \frac{23}{200}\cos\left(\frac{2\pi}{P}2n\right) \tag{12}$$

$w_{new}(n)$ has been plotted in Fig. 6, it can be seen that the new window, $w_{new}(n)$, has narrower main lobe width compared with that of the traditional Hanning or Hamming windows. Furthermore, the main lobe width of the new window,

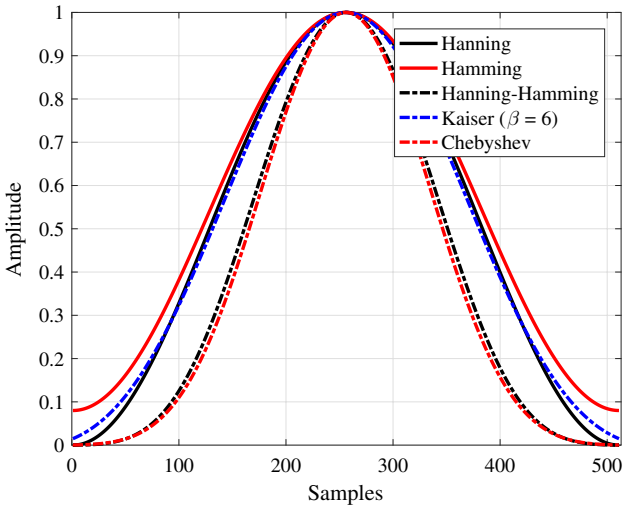

Fig. 6 Hanning–Hamming window comparison with Hanning, Hamming, Kaiser, and Chebyshev windows in the frequency domain

labeled as Hanning–Hamming, is near to the main lobe width of the Chebyshev window and narrower than that of the Kaiser window, where the controlling parameter of the Kaiser window $\beta = 6$, which will be discussed later. On the other hand, the frequency domain realization can be seen in Fig. 7, which depicts the performance of Hanning–Hamming

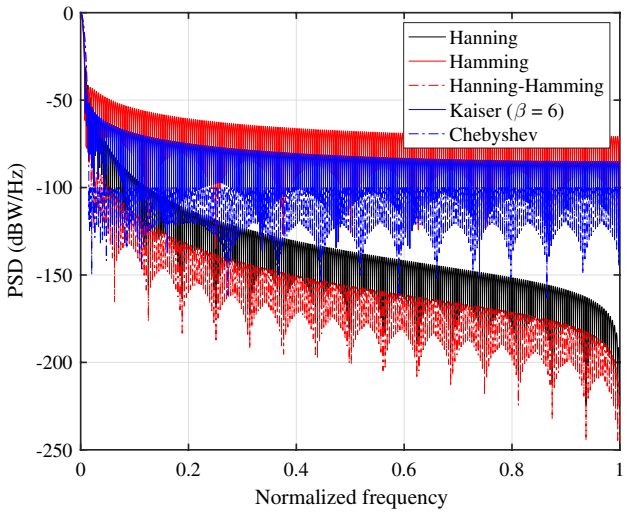

Fig. 7 Frequency domain comparison between Hanning–Hamming, Hanning, Hamming, Kaiser, and Chebyshev windows

window compared with Hanning, Hamming, Kaiser, and Chebyshev windows in the frequency domain.

It is shown in Fig. 7 that Hanning–Hamming window has the lowest levels of side lobes compared with that of traditional Hanning, Hamming, Kaiser, and Chebyshev windows. Figure 7 can be reproduced using the frequency domain mathematical formulation of Hanning–Hamming window,

$$W_{new}(\omega) = \frac{77}{200}\Lambda(\omega) - \frac{1}{4}\left[\delta\left(\omega - \frac{2\pi}{P}\right) + \delta\left(\omega + \frac{2\pi}{P}\right)\right] + \frac{23}{400}\left[\delta\left(\omega - \frac{4\pi}{P}\right) + \delta\left(\omega + \frac{4\pi}{P}\right)\right] \tag{13}$$

where

$$\Lambda(\omega) = e^{j\frac{\omega}{2}}\frac{\sin\left(\frac{P\omega}{2}\right)}{\sin\left(\frac{\omega}{2}\right)} \tag{14}$$

Thus, there is a Dirichlet kernel, $\Lambda(\omega)$, at the origin, which is the transform of the constant 77/200, see (12), and two pairs of the shifted kernel, as the transform of the single cycle of the two cosine pairs in (12). Furthermore, note that the first translated pair, $[\delta(\omega - 2\pi/P) + \delta(\omega + 2\pi/P)]$, are positioned in the first two zeros locations around the origin of the central-kernel, and the second pairs, $[\delta(\omega - 4\pi/P) + \delta(\omega + 4\pi/P)]$, located on the next two zeros around the central kernel. Because of each pair has opposite phase to the central-kernel, then, the first pair will cancel the side lobe of the central-kernel when they are algebraically summed, while the second pair tries to cancel the second side lobe of the central-kernel. In addition, note that the summation of all the coefficients in (12) [77/200, −0.5, and 23/200] is zero, which is an important condition to construct the accepted window's performance (Harris 1978). Various combinations can be achieved as shown in Figs. 8 and 9, where a frequency domain convolution of Kaiser window, $\beta = 6$, and Hamming window was conducted, the resultant window gave the name Kaiser–Hamming window, shows better behaviour as than that of Kaiser or Hamming windows themselves, where Kaiser–Hamming now has main lobe width slightly wider than Chebyshev window's main lobe. Note that not all combinations bring out good or accepted windows as indicated in (Harris 1978).

The second scenario can be realized by convolving a window with itself, $w_a(n) = w_b(n) = w(n)$. Such an example was

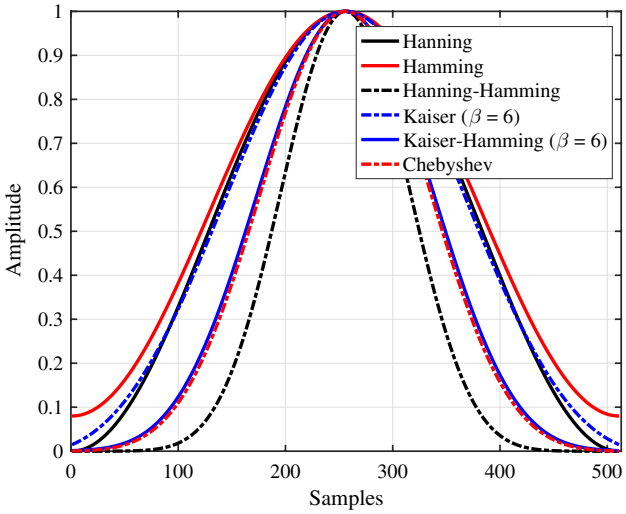

Fig. 8 Hanning–Hamming, Kaiser-Hamming, Hanning, Hamming, Kaiser, and Chebyshev windows comparison in the time domain

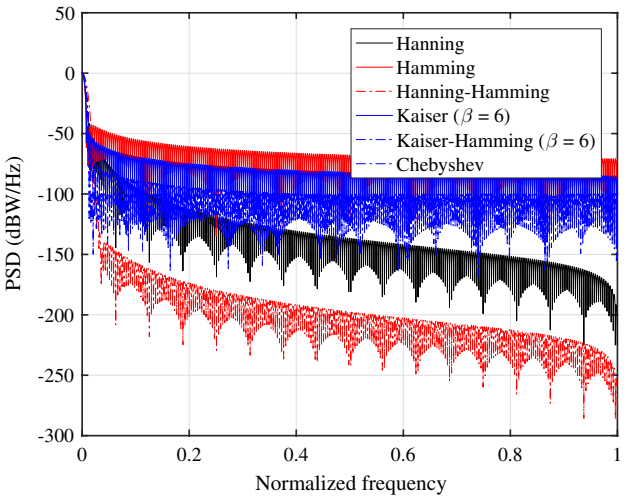

Fig. 9 Hanning–Hamming, Kaiser-Hamming, Hanning, Hamming, Kaiser, and Chebyshev windows comparison in the frequency domain

found in the literature, which is the convolution of rectangular window with itself to get the triangular In this paper, the realization of this scenario will be conducted using a Hanning window,

$$W_{new}(\omega) = W_a\left(\frac{\omega}{2}\right) * W_a\left(\frac{\omega}{2}\right) \tag{15}$$

where $\omega/2$ stands for the half−extent window. In the time domain, $w_{new}(n)$ becomes,

$$w_{new}(n) = \frac{3}{8} - \frac{1}{2}\cos\left(\frac{2\pi}{P}n\right) + \frac{1}{8}\cos\left(\frac{2\pi}{P}2n\right] \tag{16}$$

where $n = 0, 1 \cdots P$. Figure 10 presents the time domain behaviour of $w_{new}(n)$, which will be called Hanning–Hanning window, compared with Hanning, Hamming, Kaiser, and Chebyshev windows. It is obviously shown that the proposed combination, Hanning–Hanning, outperforms all other windows and follows up the same attitude of the Chebyshev window. In the frequency domain, see Figure 11, Hanning–Hanning window outperforms all windows including the Chebyshev window in terms of very high attenuation level around the two sides of the main lobe width. Actually, Hanning–Hanning window is not a new window produced in this paper, it is known in the literature as $\cos^{\alpha}(x)$ window family (Harris 1978). The frequency domain analysis of Hanning–Hamming window can be reflected to Hanning–Hanning

Nevertheless, three new windows will be constructed according to the aforementioned theory. First window will be generated by convolving Kaiser with Hanning , which will be addressed as Kaiser–Hann window, the second is obtained by the convolution of Kaiser Window with Chebyshev , and the third constructed by convolving Chebyshev

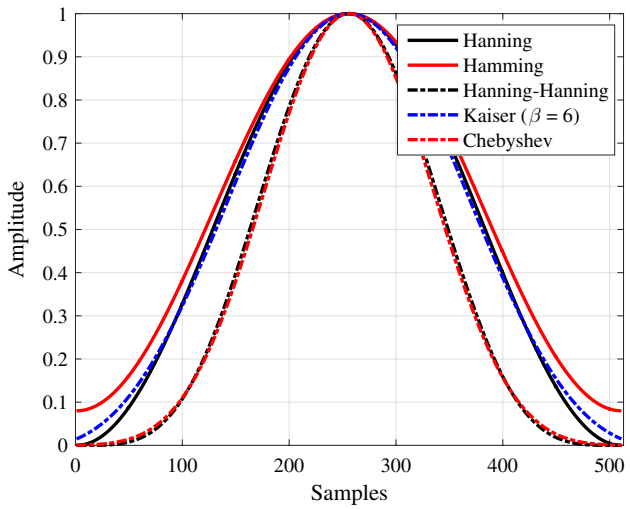

Fig. 10 Time domain comparison of Hanning–Hannig, Hanning, Hamming, Kaiser, and Chebyshev windows

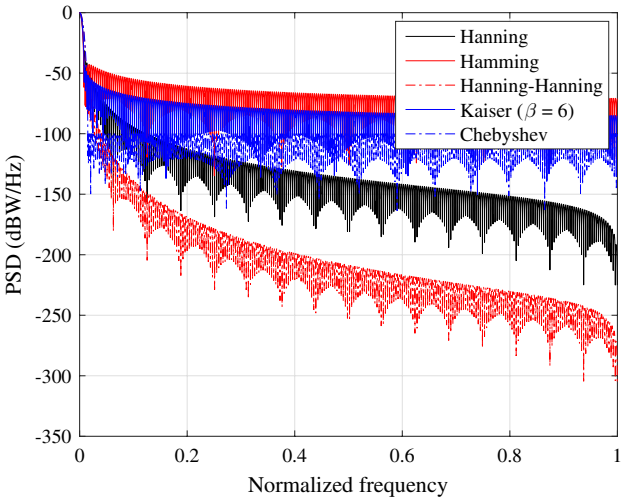

Fig. 11 Frequency domain comparison of Hanning–Hannig, Hanning, Hamming, Kaiser, and Chebyshev windows

window with itself. That is, to generate the first, which is the combination of Kaiser and Hanning windows, we start with the formulation of Kaiser Window (Kuo and Kaiser 1966)

$$w(n) = \frac{I_0(\zeta)}{I_0(\eta)} \tag{17}$$

where $I_0(x)$ is the zero-order modified Bessel function given as,

$$I_0(x) = \sum_{k=0}^{\infty}\left[\frac{\left(\frac{x}{2}\right)^k}{k!}\right]^2 \tag{18}$$

and

$$\zeta = \beta\pi\sqrt{1 - \left(\frac{n}{P/2}\right)^2} \tag{19}$$

$$\eta = \beta\pi \tag{20}$$

where η stands for the half time-bandwidth product. That is, the frequency domain representation can be, approximately, formulated as (Harris 1978)

$$W(\omega) = \frac{P}{I_0(\eta)}\frac{\sinh\left[\sqrt{\eta^2 - \left(\frac{P\omega}{2}\right)^2}\right]}{\sqrt{\eta^2 - \left(\frac{P\omega}{2}\right)^2}} \tag{21}$$

in the above expressions, (19)–(21), the parameter β controls the main lobe width and side lobe levels. For the sake

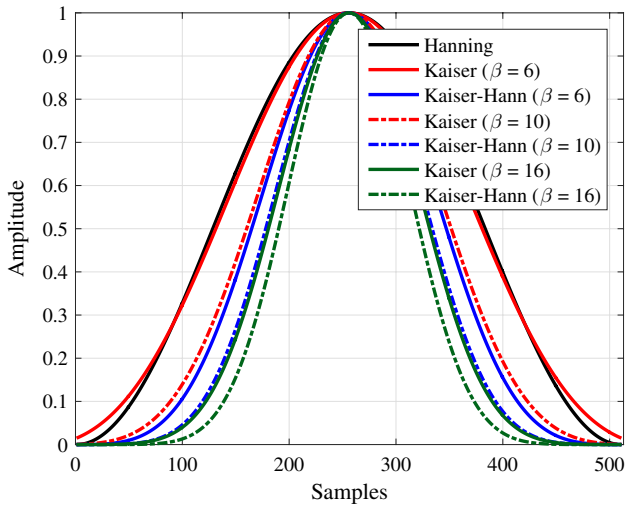

Fig. 12 Comparison between Kaiser–Hann, Hanning, and Kaiser windows for different values of the controlling factor β in the time domain

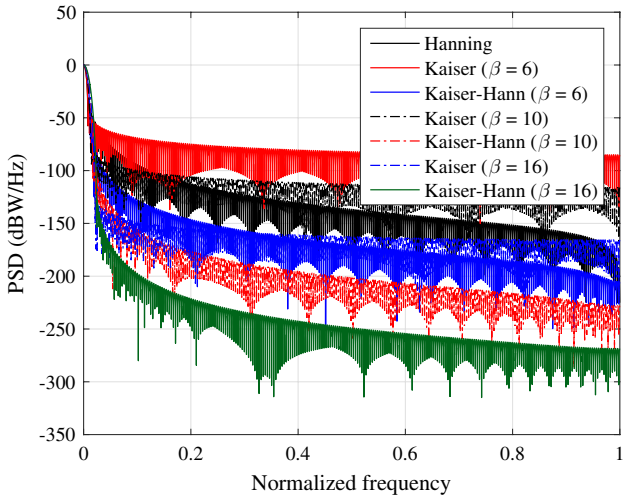

Fig. 13 Comparison between Kaiser−Hann, Hanning, and Kaiser windows for different values of the controlling factor β in the frequency domain

of simplicity, the product of Kaiser Window with Hanning will be utilized in the time domain, which corresponds for convolution in the frequency domain,

$$w(n) = \frac{I_0(\zeta)}{2I_0(\eta)}\left[1 - \cos\left(\frac{2\pi}{P}n\right)\right] \tag{22}$$

then, the resultant window has only one controlling factor, which is β. Kaiser–Hann window is shown in Fig. 12, where a comparison with Kaiser and Hanning windows in the time domain, while the corresponding frequency domain comparison is drawn in Fig. 13.

Thus, with controlling factor $\beta = 6$, the Kaiser window performs, almost, like the Hanning window, while Kaiser–Hann with the same controlling factor performs slightly better than Kaiser window, which has larger controlling factor i.e., increased complexity, $\beta = 10$. This combination, then, reduced the complexity of the traditional Kaiser window. Moreover, Kaiser–Hann of $\beta = 10$ has an identical performance of the conventional Kaiser window of $\beta = 16$. Last but not least, when $\beta = 16$ Kaiser–Hann outperforms all the cases of β as shown in Fig. 12. The same scenario of Fig. 12 can be tracked in Fig. 13 but in the frequency domain, Kaiser–Hann of $\beta = 16$ outperform all the cases of β with minimum side-lobe levels.

The second proposed window is the time domain product, which corresponds to convolution in the frequency , of Kaiser Window by Chebyshev . The Dolph–Chebyshev window formulation in the frequency domain can be written as (Helms 1971),

$$W(k) = (-1)^k \frac{\cos(\psi)}{\cosh(\gamma)} \tag{23}$$

where $0 \le k \le P-1$,

$$\psi = \cos\left[P\cos^{-1}\left[\rho\cos\left(\pi\frac{k}{P}\right)\right]\right] \tag{24}$$

$$\gamma = \cosh\left[P\cosh^{-1}(\rho)\right] \tag{25}$$

while the time domain formulation is (Andreas 2006)

$$w(n) = \frac{1}{P}\left[\rho^{-1} + 2\sum_{i=1}^{(P-1)/2} T_{P-1}\left(x_o\cos\left(\frac{i\pi}{P}\right)\right)\cos\left(\frac{i2\pi}{P}n\right)\right] \tag{26}$$

where $n = 0, 1\cdots(P-1)/2$, ρ is the passband ripple,

$$x_o = \cosh\left(\frac{1}{P-1}\cosh^{-1}\left(\rho^{-1}\right)\right) \tag{27}$$

and

$$T_k(x) = \begin{cases} \cos\left(k\cos^{-1}(x)\right), & -1 \le x \le 1 \\ \cosh\left(\cosh^{-1}(x)\right), & -1 < x < 1. \end{cases} \tag{28}$$

In (28), $T_k(x)$ stands for the k^{th}−order Chebyshev polynomial. Thus, by convolving a half-extent of (23) with the half-extent of (21), the Kaiser–Cheby window will be obtained. Two controlling parameters arise, the first one is β, due to Kaiser Window, and the second parameter is ρ, due to Chebyshev window. In Fig. 14, three values for β will be investigated, $\beta = [6, 10, 16]$, while ρ will be selected to produce $-100dB$ stop-band attenuation for all cases of β. It is evident in Fig. 14 that Kaiser–Cheby window, considering $\beta = 6$, has the same attitude as that of Kaiser window but when $\beta = 16$, thus, a dramatic complexity reduction is recognized. Furthermore, when $\beta = 10$ in Kaiser–Cheby window, the

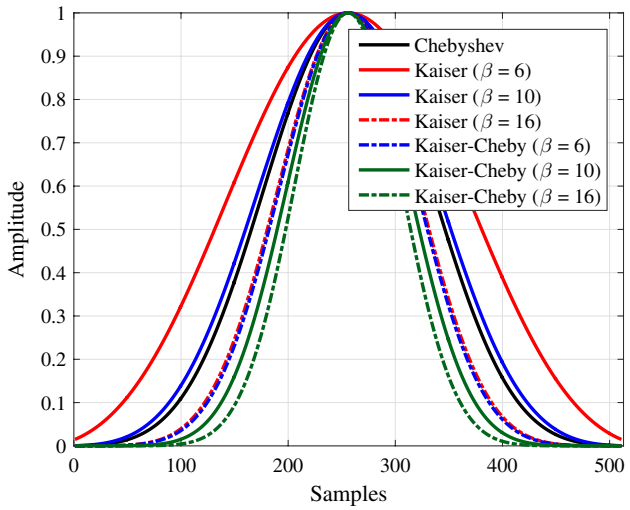

Fig. 14 Time domain comparison of Kaiser–Cheby window with Kaiser and Chebyshev windows for different values of β and $\rho = 100$

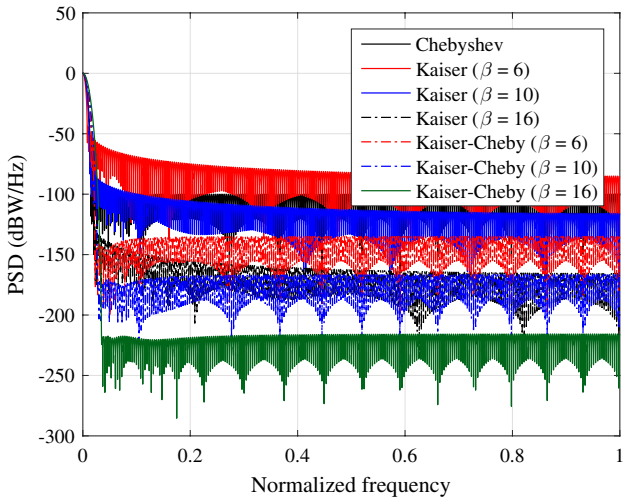

Fig. 15 Frequency domain comparison of Kaiser–Cheby window with Kaiser and Chebyshev windows for different values of β and $\rho = 100$

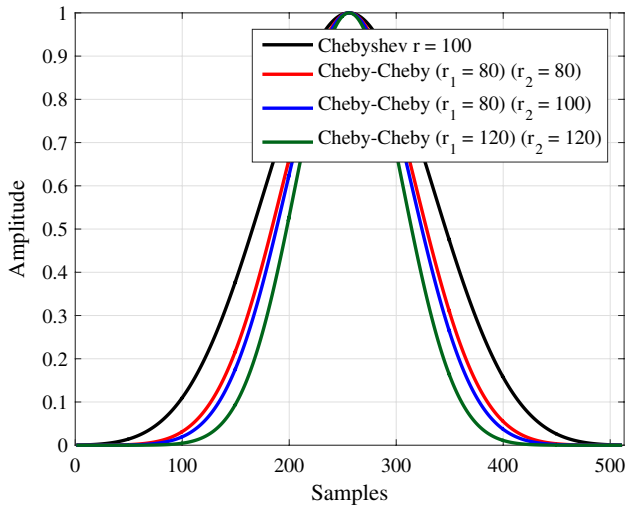

Fig. 16 Cheby–Cheby window compared with the traditional Chebyshev for different values of the stop-band controlling parameter in the time domain

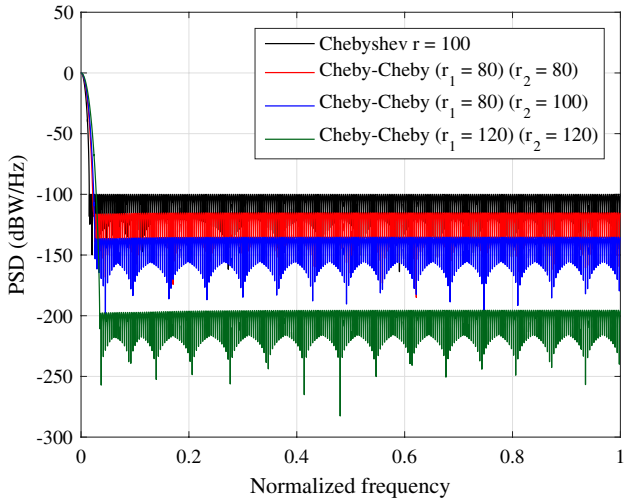

Fig. 17 Cheby–Cheby window compared with the traditional Chebyshev for different values of the stop-band controlling parameter in the frequency domain

results outperform the Kaiser window when $\beta = 16$, again, significant complexity reduction was achieved. The same performance of Kaiser–Cheby window in the frequency domain was accomplished as shown in Fig. 15, where it is obviously shown that when $\beta = 10$, Kaiser–Cheby window has higher stop-band attenuation level compared with that of the traditional Kaiser window when $\beta = 16$. Furthermore, when $\beta = 16$, Kaiser–Cheby window outperforms all other cases.

The last proposed window is the result of convolving Chebyshev window with itself. Or by multiplying (28) by itself. The new window will be called Cheby–Cheby window. The only one controlling parameter is ρ, which will be varied as shown in Fig. 16 and 17. In Fig. 16, the traditional Chebyshev window is compared with three cases of the Cheby–Cheby window, where the traditional Chebyshev has $\rho = 100dB$ down the main lobe, while the three cases are organized as; case 1, Cheby–Cheby window with controlling parameter for the first and second Chebyshev window, i.e., $w_a(n)$ and $w_b(n)$, $\rho = 80dB$, case 2, the fires Chebyshev window has $\rho = 80dB$ and the second Chebyshev window has $\rho = 100dB$, the third case is that the first and second Chebyshev windows have the same controlling parameter value, $\rho = 120dB$. The performance of the first Cheby–Cheby window, $\rho_1 = \rho_2 = 80dB$, is near to the performance of second

case, i.e., when $\rho_1 = 80dB$ and $\rho_2 = 100dB$, while the last case, $\rho_1 = \rho_2 = 120dB$, outperforms all previous cases. In Fig. 17, the best attitude was captured when controlling parameters, ρ_1 and ρ_2, equal to $120dB$ down the main lobe.

Having the prototype filter being designed, it can be employed as the filter block in the transceiver diagram of Fig. 5a, for the Tx side, and Fig. 5b, for the Rx side, respectively. The next section demonstrates the detailed results when the suggested windows are integrated into the system.

5 Results and discussions

Various windows were introduced in the last section, in this section three windows will be examined, Kaiser–Hann, Kaiser–Cheby, and Cheby–Cheby windows, where they will be employed to generate the filters. Hence, by considering the soft truncating (Abdoli et al. 2015) of a prototype filter, which will be a rectangular frequency response prototype filter, using a window function. The time domain correspondence to rectangular filter is sinc−function $p(n)$

$$f(n) = p(n) \cdot w(n) \tag{29}$$

where $w(n)$ is any one of our suggested three windows demonstrated in the last section. This section consists of three scenarios; the first scenario uses Kaiser–Hann window, second scenario employes Kaiser–Cheby window, while the last scenario utilizes the Cheby–Cheby window. Table 2 lists the most important simulation parameters for the first scenario. There will be an acceptable number of Monte–Carlo iterations to get accurate performances (Schwarz and Rupp 2016; Schwarz et al. 2017) as demonstrated in Table 2. The experiments will be conducted using Kaiser, Hanning, and Kaiser-Hann windows. Kaiser main-lobe width and side lobe level controlling parameter, β will be adopted as 6, 10, and 16 respectively, for the comparison purposes. Further, the F-OFDM symbol size will be 1024 subcarriers, accordingly,

Table 2 Simulation parameters of the first scenario

Parameter	Setting(s)
Window	Kaiser, Hanning, Kaiser–Hann
β	6, 10, 16
I/FFT size	1024
Filter Length (L)	(IFFT size)/2 − 1 = 511
Cyclic Prefix length (CP)	72
Bits per subcarrier	6, 8
Resource Blocks (RBs)	50
subcarriers per RB	12
Tone offset (excess bandwidth)	2.5
Monte–Carlo iterations	50, 000

the filter size will be 511 points when the cyclic prefix is 72 subcarriers. In each subcarrier there will be 6-bits or 8-bits as loading data, i.e. the modulation order is 64-QAM and 256-QAM, respectively. Moreover, the simulation conducted for 50 RBs, where each RB holds 12 subcarriers. The ramp up/down transition (tone-offset or excess bandwidth) will be 2.5 subcarriers. On the other hand, the number of Monte-Carlo iterations are 50,000 (Schwarz and Rupp 2016; Schwarz et al. 2017) as shown in Table 2.

To compose asynchronous communications with mixed numerology, the OOB emission should be reduced significantly to an extent level, so as to prevent the interference. Exploiting the parameters exhibited in Table 2, the block diagrams presented in Fig. 5a, b can be implemented.

Hence, Figure 18 demonstrated the results of the first scenario for 64−QAM F-OFDM. It is revealed in Fig. 18 that the power spectral density (PSD) of the F-OFDM, which is based on Kaiser–Hann window based filtering operation, has improved performance. For instance, when $\beta = 6$, the traditional Kaiser window-based filter produces F-OFDM PSD superior to that of the traditional CP-OFDM. The sidelobe levels of the traditional Kaiser window based F-OFDM, clearly started at $-140\,dB$, while the system based on Kaiser–Hann with the same β shows an enhancement by about $50\,dB$. However, since β is too small, Hanning based system still outperforms that based on Kaiser–Hann by $15\,dB$. Empowering β to be 10, the PSD based Kaiser–Hann filter shows a stop-band attenuation level of $-230\,dB$, which is compared with the traditional PSD based Kaiser window, it produces improvement by $65\,dB$. Furthermore, when $\beta = 10$, Kaiser–Hann based system outperforms the Hanning based system by more than $75\,dB$. Moreover, setting up β to 16 in

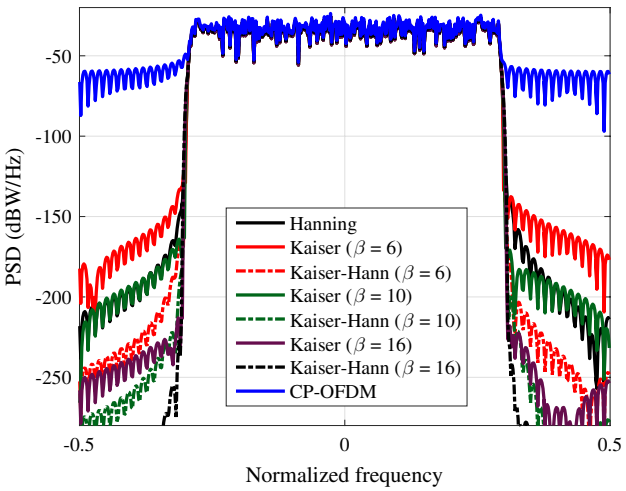

Fig. 18 Power spectral density performance evaluation of F-OFDM based Hanning, Kaiser, Kaiser–Hann windows with various β values compared with the traditional CP-OFDM for the 64−QAM mapping order

the Kaiser–Hann window, the stop-band attenuation level outperforms all the previous settings, where the side lobes appeared at $-265\,dB$.

The synchronization problems due to influence by physical components of the filter is now relaxed since we relaxed the synchronization for asynchronous communication. The bit error rate (BER) of the current scenario is shown in Fig. 19. It is shown that the worse performance is due to the CP-OFDM, while the BER performance based on Kaiser–Hann shows the best BER but at the expense of the degradation in PSD performance. When $\beta = 6$, the BER of Kaiser–Hann based system outperforms the CP-OFDM and Kaiser based system (when $\beta = 10$), but again, at the cost of PSD performance degradation. Last but not least, when $\beta = 16$, the BER performance of Kaiser–Hann and Kaiser based systems, are identical to each other and both outperform the traditional CP-OFDM system.

Additionally, to increase the capacity once more, the baseband mapping can be increased from 64−QAM to 256−QAM. Figures 20 and 21 show the PSD and BER curves of the 256−QAM based F-OFDM using Kaiser–Hann window compared with the traditional Kaiser and Hanning based F-OFDM signals. The stop-band attenuation almost did not affected by the increment of baseband mapping order, as shown in Fig. 20, than that shown in Fig. 18, but the side-lobe ripples have lower levels. Moreover, the BER performance of the proposed window is identical to the traditional Hanning and Kaiser windows as well the C-OFDM, as shown in Fig. 21.

Nevertheless, the second scenario is based on the Kaiser–Cheby window to generate the F-OFDM signals. Table 3 indicates the adopted simulation parameters for this scenario. The parameters indicated in Table 3 are identical to that of Table 2 but now we included the stopband attenuation factor, $\rho = 100dB$, which is related to Chebyshev window which will be employed in this scenario. Employing the parameters of Table 3, three cases will be shown in this scenario; the first case is based on $\beta = 6$, second case based on $\beta = 10$, and the last case when $\beta = 16$, where these three cases will be implemented two times, the first time utilize 64−QAM and the second time will be based on 256−QAM. Figure 22 shows the PSD of the 64−QAM F-OFDM based Kaiser–Cheb window filtering, for the three cases compared

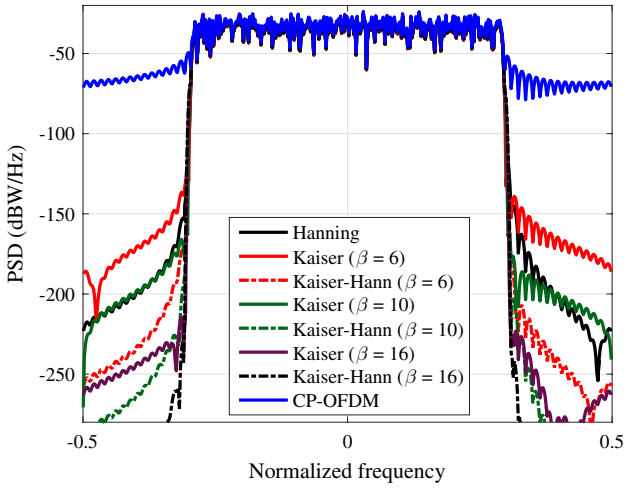

Fig. 20 Power spectral density performance evaluation of F-OFDM based Hanning, Kaiser, Kaiser–Hann windows with various β values compared with the traditional CP-OFDM for the 256−QAM mapping order

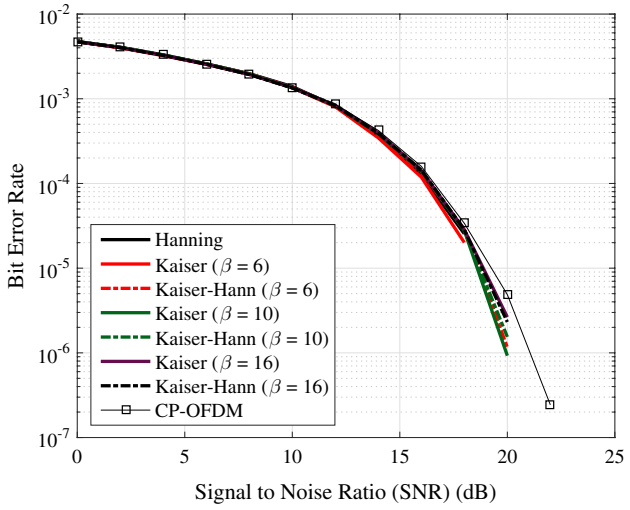

Fig. 19 Bit error rate performance evaluation of F-OFDM based Hanning, Kaiser, Kaiser–Hann windows with various β values compared with the traditional CP-OFDM for the 64−QAM mapping order

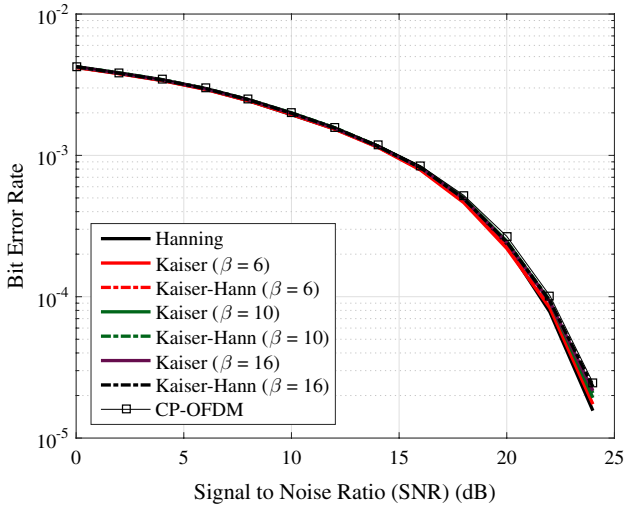

Fig. 21 BER evaluation of F-OFDM based Hanning, Kaiser, Kaiser–Hann windows with various β values compared with the traditional CP-OFDM for the 256−QAM mapping order

Table 3 Simulation parameters of the second scenario

Parameter	Setting(s)
Window	Kaiser, Chebyshev, Kaiser–Cheby
β	6, 10, 16
ρ	100dB down the main lobe level
I/FFT size	1024
Filter length (L)	(IFFT size)/2 − 1 = 511
Cyclic prefix length (CP)	72
Bits per subcarrier	6, 8
Resource blocks (RBs)	50
Subcarriers per RB	12
Tone offset (excess bandwidth)	2.5
Monte–Carlo iterations	50, 000

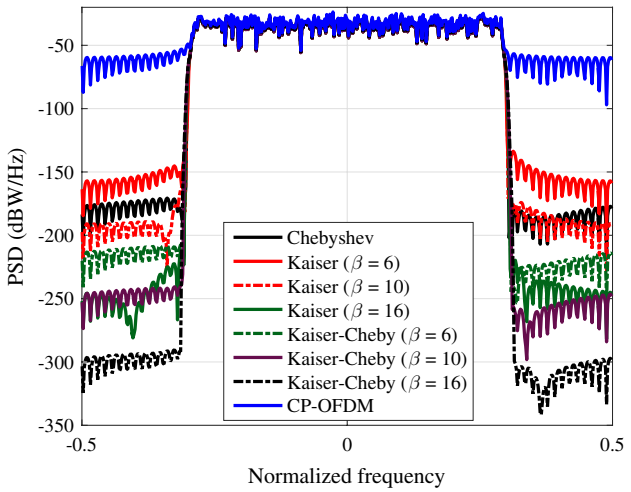

Fig. 22 Power spectral density performance evaluation of 64–QAM F-OFDM based Chebyshev, Kaiser, Kaiser–Cheby windows with various β values compared with the traditional 64–QAM CP-OFDM

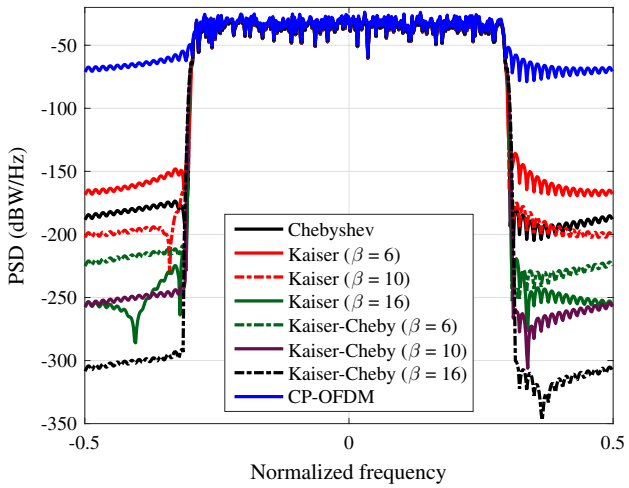

Fig. 23 Power spectral density performance evaluation of 256–QAM F-OFDM based Chebyshev, Kaiser, Kaiser–Cheby windows with various β values compared with the traditional 256–QAM CP-OFDM

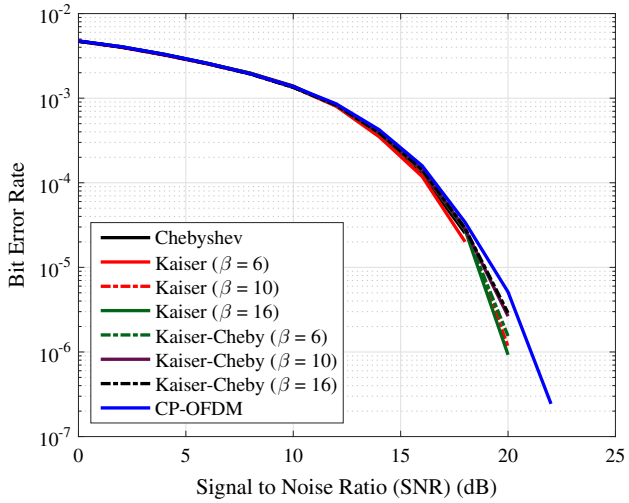

Fig. 24 BER performance evaluation of 64–QAM F-OFDM based Chebyshev, Kaiser, Kaiser–Cheby windows with various β values compared with the traditional 64–QAM CP-OFDM

with the three cases of Kaiser based systems and Chebyshev compared with the CP-OFDM system. It is shown that F-OFDM based Kaiser–Cheby window, using $\beta = 6$, outperforms that one based on Kaiser window by 15 dB, but when $\beta = 10$, the Kaiser and Chebyshev based systems have, approximately, the same performance. When $\beta = 16$, the Kaiser based system superior the previously conducted procedures. However, the Kaiser–Cheby window with $\beta = 6$ and $\rho = 100\,dB$, which is fixed in this scenario, the performance improved by 45 dB, 65 dB, and 70 dB, with respect to Chebyshev, Kaiser ($\beta = 10$), and Kaiser window ($\beta = 6$), respectively, as well as the conventional CP-OFDM. Furthermore, if β increased, $\beta = 10$, then the PSD behaviour of the F-OFDM based Kaiser–Cheby window beats the previous settings, which shows a stop-band level down to −250 dB. Moreover, employing $\beta = 16$, the stop-band attenuation reaches −300 dB. Such significant superior attenuation level helps the system to be perfectly deployed with mixed numerology. In Fig. 23, the same results explored in Fig. 22 are obtained but with 256–QAM based F-OFDM system, i.e., there are 8 bits per each sub-carrier rather than 6 bits per subcarrier.

On the other hand, the BER performance of the 64–QAM based Kaiser–Cheby F-OFDM signal is shown in Fig. 24. Thus, in Fig. 24, the BER performance of the conventional CP-OFDM indicates more power is required, while Chebyshev, Kaiser, and Kaiser–Cheby based F-OFDM signals show improved BER. Although there is a slight improvement in the BER of the Kaiser based system, when $\beta = 16$,

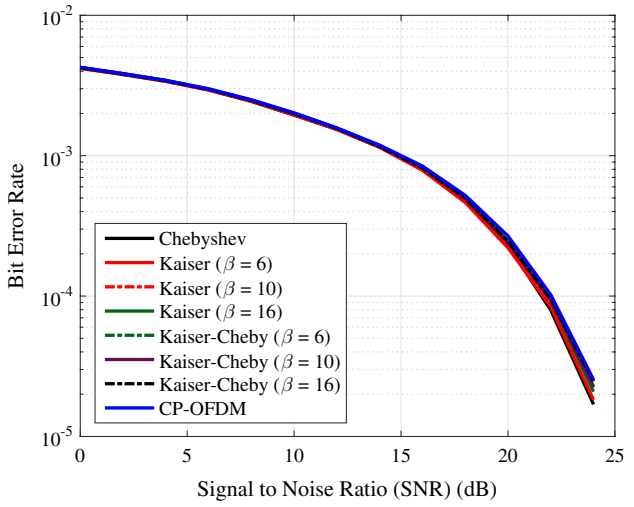

Fig. 25 BER performance evaluation of 256–QAM F-OFDM based Chebyshev, Kaiser, Kaiser–Cheby windows with various β values compared with the traditional 256–QAM CP-OFDM

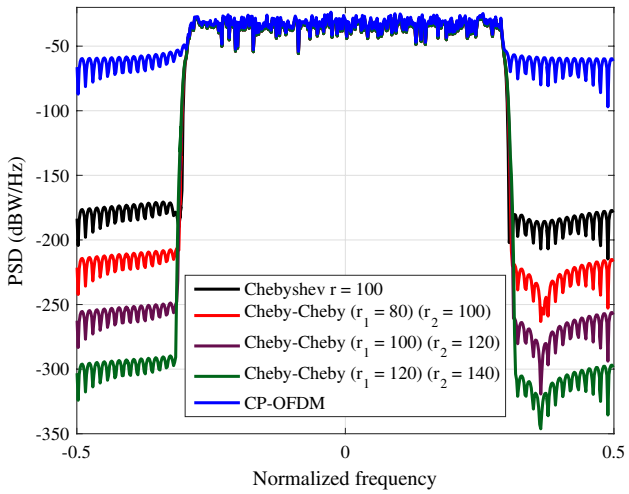

Fig. 26 Power spectral density performance evaluation of 64–QAM F–OFDM based Chebyshev, Cheby–Cheby windows with various attenuation factor values compared with the traditional 64–QAM CP-OFDM

Table 4 Simulation parameters of the third scenario

Parameter	Setting(s)
Window	Chebyshev, Cheby–Cheby
ρ	100dB down the main lobe level
Case #1 (ρ_1, ρ_2)	(80, 80)
Case #2 (ρ_1, ρ_2)	(80, 100)
Case #3 (ρ_1, ρ_2)	(120, 140)
I/FFT size	1024
Filter length (L)	(IFFT size)/2 − 1 = 511
Cyclic prefix length (CP)	72
Bits per subcarrier	6, 8
Resource blocks (RBs)	50
Subcarriers per RB	12
Tone offset (excess bandwidth)	2.5
Monte–Carlo iterations	50, 000

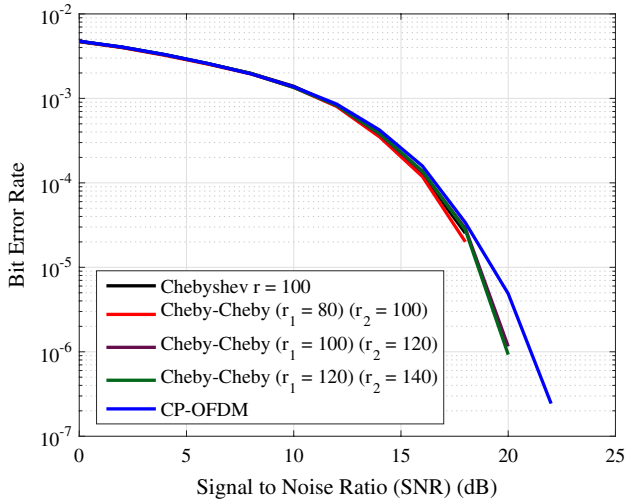

Fig. 27 BER comparison of 64–QAM F-OFDM based Chebyshev, Cheby–Cheby windows with various attenuation factor values compared with the traditional 64–QAM CP-OFDM

the PSD performance is poor. In Fig. 25, it is obvious that the BER performances of all of the previous cases, but when the baseband mapping becomes 256–QAM, have an approximately identical shape along the signal-to-noise ratio values.

The same parameters of Table 3 are conducted for the third scenario, thus, last but not least, Table 4 puts on view the simulation parameters for the third scenario. The third assumption will be developed on the bases of Cheby–Cheby window. Only one parameter is related to the Chebyshev , but the suggested Cheby–Cheby window can still use two attenuation levels individually for the sake of more flexibility. The same strategies developed in the last two scenarios have been used to develop the third scenario, where the PSD and BER performances of the F-OFDM based on Chebyshev ($\rho = 100\,dB$), Cheby–Cheby ($\rho_1 = 80\,dB, \rho_2 = 100\,dB$), Cheby–Cheby ($\rho_1 = 100\,dB, \rho_2 = 120\,dB$) , and Cheby–Cheby ($\rho_1 = 120\,dB, \rho_2 = 140\,dB$) using 64–QAM mapping, are shown in Figs. 26 and 27, respectively. While the 256–QAM PSD and BER results are shown in Figs. 28 and 29, respectively. That is, in Fig. 26, the PSD of F-OFDM based Chebyshev window filtering outperforms the conventional CP-OFDM by 125 dB, while that system based on Cheby–Cheby (first case in Table 4) outperforms the later by 50 dB. Furthermore, when $\rho_1 = 100dB$ and $\rho_2 = 120\,dB$,

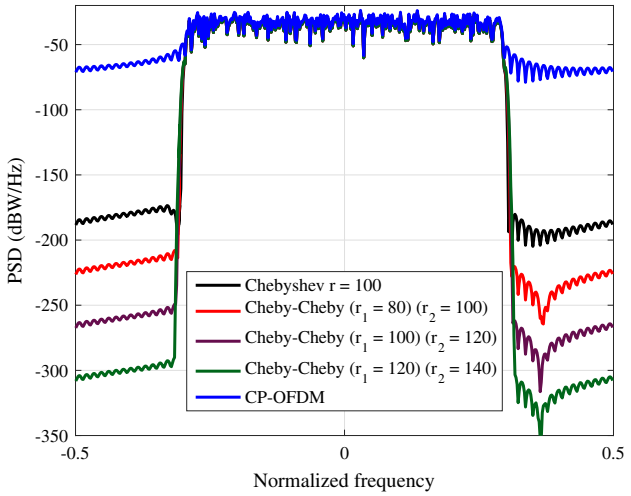

Fig. 28 Power spectral density performance evaluation of 256−QAM F-OFDM based Chebyshev, Cheby–Cheby windows with various attenuation factor values compared with the traditional 256−QAM CP-OFDM

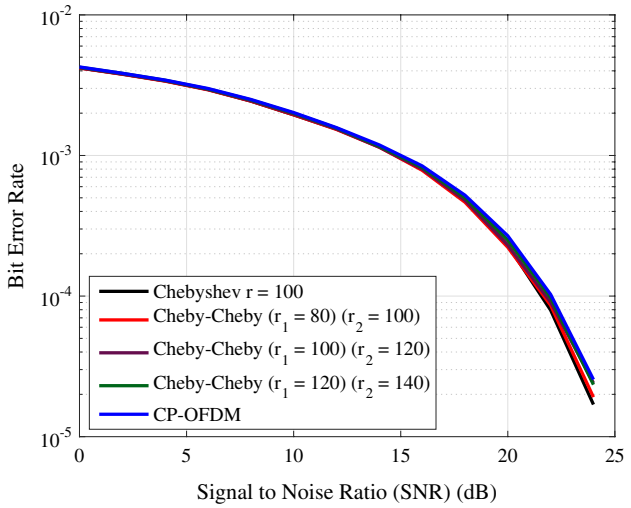

Fig. 29 BER comparison between 256−QAM F-OFDM based Chebyshev, Cheby–Cheby windows with various attenuation factor values compared with the traditional 256−QAM CP-OFDM

the performance enhanced by 200 dB, 75 dB, and 50 dB with respect to CP-OFDM, Chebyshev, and Cheby–Cheby when $\rho_1 = 80\,dB$ and $\rho_2 = 100\,dB$, respectively. Moreover, when $\rho_1 = 120\,dB$ and $\rho_2 = 140\,dB$, the improvement becomes dramatic with respect to all of the previous cases, where the stop-band attenuation level drops down to $-300\,dB$

The BER performance corresponds to the results in Fig. 26 is given in Fig. 27. It can be observed in Fig. 27 that the worse BER performance belongs to the CP-OFDM, which is required more transmission power, while the system based on Cheby–Cheby, when $\rho_1 = 80\,dB$ and $\rho_2 = 100\,dB$, represents an improvement but at the expense of the PSD degradation behavior. The system based on Cheby–Cheby or $\rho_1 = 120\,dB$ and $\rho_2 = 140\,dB$ shows the superior performance. Figure 28 displays the PSD of the F-OFDM based on the suggested window, Cheby–Cheby, using the same settings of Fig. 26 but by employing 256−QAM mapping. It is shown in Fig. 28 that the same findings obtained due to 64−QAM are attained again, where the best performance was obtained using Cheby–Cheby when $\rho_1 = 120\,dB$ and $\rho_2 = 140\,dB$. On the other hand, the BER of the corresponding findings of Fig. 28 can be recognized in Fig. 29. The BER performance of all the previous cases based on Chebyshev, Cheby–Cheby of 256−QAM, are almost identical to each other, as well as the CP-OFDM BER performance.

Alongside the above results, theoretically, it is easy to show that the time-frequency efficiency (Bazzi et al. 2015) of the F-OFDM is improved with respect to the traditional CP-OFDM. However, Fig. 30 brings to view the difference between F-OFDM and CP-OFDM. It can be seen that CP-OFDM with less number of sub-carriers with respect to the F-OFDM, has lower efficiency. For instance, when the number of sub-carriers is 80, the CP-OFDM time-frequency efficiency is 30%, while F-OFDM approximately equals to 93%. Thus, F-OFDM outperforms the CP-OFDM and can be agreed for the next generation of communication systems.

6 Conclusion

To achieve improvements in the requirements of the 5G systems with mixed numerology, a synchronization free communications is required. F-OFDM is one of the promising waveform candidates to this goal. Various filter designs have

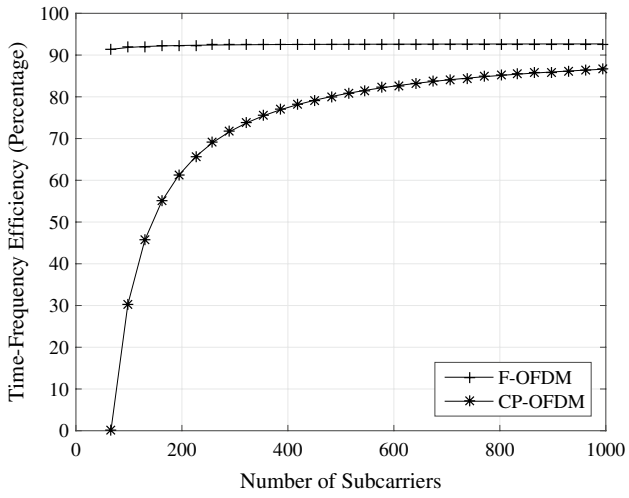

Fig. 30 Time-Frequency efficiency comparison between F-OFDM and CP-OFDM systems

been introduced in this paper to improve the F-OFDM wave form in terms of time-frequency localization, such that the spectral efficiency improved dramatically compared with that of the traditional CP-OFDM. The proposed designs can be implemented on-line without increased complexity, while maintaining the conventional F-OFDM structure. The new design has no limitations with respect to the size of the symbol size or the baseband modulation (Mapping order, M-QAM).

Acknowledgements The authors would like to acknowledge the help and support introduced in the Space Navigation and Control Laboratory (SNCL) of the Department of Communications Engineering, College of Engineering, University of Diyala.

Compliance with ethical standards

Conflict of interest The authors declare that they have no conflict of interest.

References

5G-NR (2019) Base station (BS) radio transmission and reception. ETSI TS.138.104: Release 15, version 15.5.0 www.etsi.org

Abdoli J, Jia M, Ma J Filtered (2015) OFDM: a new waveform for future wireless systems. In: 2015 IEEE 16th international workshop on signal processing advances in wireless communications (SPAWC), Stockholm, Sweden, 28 June-1 July. pp 66–70. https://doi.org/10.1109/SPAWC.2015.7227001

Ahmed MS, Shah NSM, Ghawbar F, Jawhar YA, Almohammedi AA (2020) Filtered-OFDM with channel coding based on T-distribution noise for underwater acoustic communication. J Amb Intel Hum Comp. https://doi.org/10.1007/s12652-020-01713-9

An C, Kim B, Ryu H (2017) WF-OFDM (windowing and filtering OFDM) system for the 5G new radio waveform. In: 2017 IEEE XXIV international conference on electronics, electrical engineering and computing (INTERCON), Cusco, Peru, August 15–18. pp 1–4. https://doi.org/10.1109/INTERCON.2017.8079635

Andreas A (2006) Digital signal processing: signals, systems, and filters. McGraw-Hill, New York

Andrews JG, Buzzi S, Choi W, Hanly SV, Lozano A, Soong ACK, Zhang JC (2014) What Will 5G Be? IEEE J SEL AREA COMM 32(6):1065–1082. https://doi.org/10.1109/JSAC.2014.2328098

Banelli P, Buzzi S, Colavolpe G, Modenini A, Rusek F, Ugolini A (2014) Modulation formats and waveforms for 5G networks: Who willbe the heir of OFDM?: an overview of alternative modulation schemes for improved spectral efficiency. IEEE Signal Proc Mag 31(6):80–93. https://doi.org/10.1109/MSP.2014.2337391

Bazzi J, Weitkemper P, Kusume K, Benjebbour A, Kishiyama Y (2015) Design and Performance Tradeoffs of Alternative Multi-Carrier Waveforms for 5G. In: 2015 IEEE globecom workshops (GC Wkshps), San Diego, December 6–10. pp 1–6. https://doi.org/10.1109/GLOCOMW.2015.7414010

Bedoui A, Et-tolba MA (2017) Comparative analysis of filter bank multicarrier (FBMC) as 5G multiplexing technique. In: 2017 international conference on wireless networks and mobile communications (WINCOM), Rabat, Morocco, November 1–4. pp 1–7. https://doi.org/10.1109/WINCOM.2017.8238200

Bellanger M et al. (2010) FBMC physical layer : a primer PHYDYAS:1–31

Bölcskei H (2003) Orthogonal frequency division multiplexing based on offset QAM. In: Feichtinger HG, Strohmer T (eds) Advances in gabor analysis, Birkhäuser Boston, Boston, pp 321–352. doi: https://doi.org/10.1007/978-1-4612-0133-5_12

Cheng X, He Y, Ge B, He C A (2016) Filtered OFDM Using FIR Filter Based on Window Function Method. In: 2016 IEEE 83rd vehicular technology conference (VTC Spring), Nanjing, China, May 15-18. pp 1–5. https://doi.org/10.1109/VTCSpring.2016.7504065

Farhang-Boroujeny B, Yuen C (2010) Cosine modulated and offset QAM filter bank multicarrier techniques: a continuous-time prospect. Eurasip J Adv Sig Pr 2010:165654. https://doi.org/10.1155/2010/165654

Fettweis G, Krondorf M, Bittner S (2009) GFDM - generalized frequency division multiplexing. In: VTC Spring 2009— IEEE 69th vehicular technology conference, Barcelona, Spain, April 26–29. pp 1–4. https://doi.org/10.1109/VETECS.2009.5073571

Gokceli S, Basar E, Kurt GK (2018) Universal filtered OFDM with filter shift keying—Invited Paper. In: 2018 IEEE 87th vehicular technology conference (VTC Spring), Porto, Portugal, June 3–6. pp 1–5. https://doi.org/10.1109/VTCSpring.2018.8417532

Hammoodi A, Audah L, Taher MA (2019) Green coexistence for 5G waveform candidates: a review. IEEE ACCESS 7:10103–10126. https://doi.org/10.1109/ACCESS.2019.2891312

Harris FJ (1978) On the use of windows for harmonic analysis with the discrete Fourier transform. P IEEE 66(1):51–83. https://doi.org/10.1109/PROC.1978.10837

Helms H (1971) Digital filters with equiripple or minimax responses. IEEE T Acoust Speech 19(1):87–93. https://doi.org/10.1109/TAU.1971.1162156

Hu KC, Armada AG (2016) SINR analysis of OFDM and f-OFDM for machine type communications. In: 2016 IEEE 27th annual international symposium on personal, indoor, and mobile radio communications (PIMRC), Valencia, Spain, September 4–8. pp 1-6. https://doi.org/10.1109/PIMRC.2016.7794702

Huawei and HiSilicon (2016) f-OFDM scheme and filter design. 3GPP RAN1 #85 Meeting, Technical Document R1–165425, Nanjing, China, May 23-27

Iwabuchi M , Benjebbour A et al. (2017) 5G field experimental trial on frequency domain multiplexing of mixed numerology. In: 2017 IEEE 85th vehicular technology conference (VTC Spring), Sydney, Australia, June 4–7. pp 1–5. https://doi.org/10.1109/VTCSpring.2017.8108645

Jawhar YA, Audah L, Taher MA, Ramli KN, Shah NSM, Musa M, Ahmed MS (2019) A Review of Partial Transmit Sequence for PAPR Reduction in the OFDM Systems. IEEE ACCESS 7:18021–18041. https://doi.org/10.1109/ACCESS.2019.2894527

Kuo FF, Kaiser JF (1966) System analysis by digital computer. Wiley, New York

Lavanya P, Satyanarayana P, Mohatram M (2020) Peak to average power ratio reduction of ZT DFT-s-OFDM signals using improved monarch butterfly optimization-PTS scheme. J Amb Intel Hum Comp. https://doi.org/10.1007/s12652-020-01940-0

Li J, Bala E, Yang R (2014) Resource block filtered-OFDM for future spectrally agile and power efficient systems. Phys Commun-Amst 11:36–55. https://doi.org/10.1016/j.phycom.2013.10.003

Li J, Kearney K, Bala E, Yang R (2015) A resource block based filtered OFDM scheme and performance comparison. In: ICT 2013, Casablanca, Morocco, May 6–8. pp 1–5. https://doi.org/10.1109/ICTEL.2013.6632084

Liu Y, Chen X, Zhong Z, Ai B, Miao D, Zhao Z, Sun J, Teng Y, Guan H (2017) Waveform design for 5G networks: analysis and comparison. IEEE Access 5:19282–19292. https://doi.org/10.1109/ACCESS.2017.2664980

Lu S, Qu D, He Y (2012) Sliding window tone reservation technique for the peak-to-average power ratio reduction of FBMC-OQAM

signals. IEEE Wirel Commun Le 1(4):268–271. https://doi.org/10.1109/WCL.2012.062512.120360
Michailow N, Matthé M, Gaspar IS, Caldevilla AN, Mendes LL, Festag A, Fettweis G (2014) Generalized frequency division multiplexing for 5th generation cellular networks. IEEE T Commun 62(9):3045–3061
Mitra SK, Kuo Y (2006) Digital signal processing: a computer-based approach, vol 2. McGraw-Hill, New York
Oppenheim AV, Schafer RW, Buck JR (2014) Discrete-time signal processing. Pearson, England
Qiu Y, Liu Z, Qu D (2017) Filtered bank based implementation for filtered OFDM. In: 2017 7th IEEE international conference on electronics information and emergency communication (ICEIEC), Macau, China, July 21–23. pp 15–18. https://doi.org/10.1109/ICEIEC.2017.8076502
Renfors M, Yli-Kaakinen J, Levanen T, Valkama M, Ihalainen T, Vihriala J (2015) Efficient Fast-convolution implementation of filtered CP-OFDM waveform processing for 5G. In: 2015 IEEE globecom workshops (GC Wkshps), San Diego, December 6–10. pp 1–7. https://doi.org/10.1109/GLOCOMW.2015.7414034
Schaich F (2010) Filterbank based multi carrier transmission (FBMC)—evolving OFDM: FBMC in the context of WiMAX. In: 2010 European wireless conference (EW), Lucca, Italy, April 12–15. pp 1051–1058. https://doi.org/10.1109/EW.2010.5483518
Schaich F, Wild T, Chen Y (2014) Waveform contenders for 5G—suitability for short packet and low latency transmissions. In: 2014 IEEE 79th vehicular technology conference (VTC Spring), Seoul, South Korea, May 18-21. pp 1–5. https://doi.org/10.1109/VTCSpring.2014.7023145
Schwarz S, Philosof T, Rupp M (2017) Signal processing challenges in cellular-assisted vehicular communications: efforts and developments within 3GPP LTE and beyond. IEEE Signal Proc Mag 34(2):47–59. https://doi.org/10.1109/MSP.2016.2637938
Schwarz S, Rupp M (2016) Society in motion: challenges for LTE and beyond mobile communications. IEEE Commun Mag 54(5):76–83. https://doi.org/10.1109/MCOM.2016.7470939
Taher AM, Ahmed MA (2015) Power envelope variation improvement of downlink LTE system using complex number manipulation approach. Diyala J Eng Sci 8(4):618–623
Taher MA (2019) Enhanced 5G Throughput Using UFMC Multiplexing. Journal of Southwest Jiaotong University 54(5):1–11
Taher MA, Mandeep J, Ismail M, Samad SA, Islam M (2014) Reducing the power envelope fluctuation of OFDM systems using side information supported amplitude clipping approach. Int J Circ Theor App 42(4):425–435. https://doi.org/10.1002/cta.1896
Taher MA, Shallal AH, Qaddoori IH (2015) Non-linearity distortion Mitigation of downlink-LTE system using modified amplitude clipping and frequency domain randomization. Diyala J Eng Sci 8(4):613–617
Taher MA, Singh MJ, Ismail M, Samad SA, Islam MT, Mahdi HF (2015) Post-IFFT-modified selected mapping to reduce the PAPR of an OFDM system. Circ Syst Signal Process 34(2):535–555. https://doi.org/10.1007/s00034-014-9868-4
Taher MA, Singh MJ, Ismail MB, Samad SA, Islam MT (2013) Reducing the PAPR of OFDM systems by random variable transformation. ETRI J 35(4):714–717. https://doi.org/10.4218/etrij.13.0212.0552
Wang J, Jin A, Shi D, Wang L, Shen H et al (2017) Spectral efficiency improvement with 5G technologies: results from field tests. IEEE J Sel Area Comm 35(8):1867–1875. https://doi.org/10.1109/JSAC.2017.2713498
Wang R, Cai J, Yu X, Jiang J (2019) Temporal-correlation-based compressive channel estimation for universal filtered multicarrier system over fast-fading channels. J Amb Intel Hum Comp 10(5):1681–1692. https://doi.org/10.1007/s12652-017-0593-2
Wang X, Wild T, Schaich F, Santos AFd (2014) Universal Filtered multi-carrier with leakage-based filter optimization. In: European wireless 2014; 20th European wireless conference, Barcelona, Spain, May 14–16. pp 1–5
Weitkemper P, Bazzi J, Kusume K, Benjebbour A, Kishiyama Y (2016) On regular resource grid for filtered OFDM. IEEE Commun Lett 20(12):2486–2489. https://doi.org/10.1109/LCOMM.2016.2572183
Wild T, Schaich F, Chen Y (2014) 5G air interface design based on Universal Filtered (UF-)OFDM. In: 2014 19th international conference on digital signal processing, Hong Kong, China, August 20–23. pp 699–704. https://doi.org/10.1109/ICDSP.2014.6900754
Wu D, Zhang X, Qiu J, Gu L, Saito Y, Benjebbour A, Kishiyama Y (2016) A Field Trial of f-OFDM toward 5G. In: 2016 IEEE Globecom Workshops (GC Wkshps), Washington, DC, December 4–8. pp 1–6. https://doi.org/10.1109/GLOCOMW.2016.7848810
Yang L, Xu Y (2017) Filtered-OFDM system performance research based on Nuttall's Blackman-Harris window. In: 2017 IEEE 17th international conference on communication technology (ICCT), Chengdu, China, October 27–30. pp 687–691. https://doi.org/10.1109/ICCT.2017.8359724
Zhang X, Jia M, Chen L, Ma J, Qiu J (2014) Filtered-OFDM - enabler for flexible waveform in the 5th generation cellular networks. In: 2015 IEEE global communications conference (GLOBECOM), San Diego, CA, USA, December 6-10, pp 1–6. https://doi.org/10.1109/GLOCOM.2015.7417854
Zhou X, Wang C, Tang R, Zhang M (2018) Channel estimation based on statistical frames and confidence level in OFDM systems. Appl Sci 8:1–16